Geophys. J. Int. (2007) **168,** 949–963 doi: 10.1111/j.1365-246X.2006.03280.x

Trajectory-based modelling of broad-band electromagnetic wavefields

D. W. Vasco

Berkeley Laboratory, University of California, Berkeley, CA 94720, *USA. E-mail: dwvasco@lbl.gov*

Accepted 2006 October 26. Received 2006 October 26; in original form 2006 January 18

SUMMARY

A trajectory-based solution of Maxwell's equations is derived using the method of multiple scales. This time-domain technique utilizes an asymptotic expansion in terms of the ratio of the wave front length-scale to the length-scale of the heterogeneity. The approach provides an alternative to an expansion in terms of frequency and allows one to model electromagnetic wave propagation over a wide frequency band. At the lower end of the frequency band, the trajectory-based solution reduces to a previously derived diffusive solution. Similarly, at higher frequencies one obtains the 'delta-like' solution associated with hyperbolic wave propagation. However, the solution is also valid at intermediate frequencies which cannot be characterized as either diffusive or hyperbolic. A numerical illustration demonstrates the importance of both conduction and displacement currents at frequencies between 10 and 100 MHz. The amplitudes computed using the trajectory-based approach compare well with analytic results for a homogeneous whole-space. Using the technique I am able to model observations from a broad-band (3–300 kHz) experiment at the Richmond Field Station in California. In addition, ground penetrating radar waveforms in the 5–200 MHz range, gathered at the Boise Hydrogeophysical Research Site, are matched using the results of a radar velocity tomogram.

Key words: asymptotic methods, electromagnetic waves, tomography.

1 INTRODUCTION

Modelling the propagation of electromagnetic fields in the Earth has long been a computational challenge. The literature on mathematical and numerical methods aimed at overcoming the computational difficulties has grown significantly over the past few decades. The various methods rely on particular assumptions or approximations and are frequently limited in their range of application. Early approaches assumed highly symmetric structures such as a homogeneous or a layered half-space (Wait 1954; Morrison *et al.* 1969; Ryu *et al.* 1970; Chew 1995). Efficient integral equation methods exist for modelling compact bodies embedded in a homogeneous or layered Earth (Parry 1969; Hohmann 1971; Tripp & Hohmann 1984; Newman *et al.* 1986). The efficiency of this approach has been improved using various approximations (Habashy *et al.* 1993; Torres-Verdin & Habashy 1994) but these methods are limited in terms of the frequency range and the allowed conductivity contrasts. Finite element and finite difference methods have been applied to the modelling of electromagnetic fields within the Earth for quite some time (Coggon 1971; Silvester & Haslam 1972; Oristaglio & Hohmann 1984). Given current computational resources, in particular a sizable cluster of networked workstations, finite element and finite difference techniques can now solve moderately large 3-D problems (Druskin & Knizhnerman 1994; Newman & Alumbaugh 1995; Alumbaugh *et al.* 1996).

Typically, electromagnetic methods are used to image the subsurface, or equivalently, to solve an inverse problem (Newman & Commer 2005). That is, one is interested in estimating an earth model which is compatible with a given set of observations. For example, because of their sensitivity to fluid properties, there is renewed interest in using electromagnetic data to characterize large-scale reservoir models and for high-resolution monitoring of environmental remediation and reservoir production (Barker & Moore 1998; Binley *et al.* 2001; Hoversten *et al.* 2003). Such inverse problems require repeated solution of the forward problem and usually involve one to several orders of magnitude more computation then is necessary to solve the forward problem. Furthermore, there is recognition of the advantages of broad-band data sets, spanning the kilo-hertz to mega-hertz frequency interval (Stewart *et al.* 1994; Becker *et al.* 1999; Frangos *et al.* 2004). Data in this frequency range are particularly suited for imaging shallow and intermediate depth heterogeneity, and for inferring both conductivity and dielectric permittivity in the subsurface (Frangos *et al.* 2004). Solving the inverse problem for a wide band of frequencies and source-receiver offsets requires considerable computation, particularly for a multidimensional model (Stewart *et al.* 1994). Such inverse problems involve a large number of unknowns and sizable data sets. As models grow in complexity and the amount of data increases, the computation requirements increase dramatically for finite element and finite differenced based inversion schemes. In such imaging problems there are significant computational advantages associated with a trajectory-based methodology (Aki & Richards 2002). For example, for a grid-based model of dimension n_x by n_y by n_z the degree of computation for a trajectory-based method scales as the

© 2007 The Author
Journal compilation © 2007 RAS

number of grid blocks intersected by the trajectory. Thus, the computation grows roughly as $\sqrt{n_x{}^2 + n_y{}^2 + n_z{}^2}$. In comparison, for most finite-difference methods the required computation grows as $n_x \cdot n_y \cdot n_z$. Note that the computational savings discussed here refer to the forward problem, the computation of the field at an observation point.

There may also be some additional computational and conceptional advantages in using the approach to solve the inverse problem. The primary saving is due to the availability of analytic or semi-analytic sensitivities which relate perturbations in model parameters to perturbations in the observed field quantities. Typically such sensitivities require less computation and much less storage than do numerically derived sensitivities. The computational advantage can be reduced by the use of the adjoint form of Maxwell's equations (Newman & Commer 2005) in the numerical calculations. However, even with the use of adjoint-state methods, two forward problems must be solved in order to compute sensitivities. A conceptual advantage is provided by the fact that trajectory-based approach partitions the inverse problem into a kinematic, or arrival time matching subproblem, and a dynamic, or amplitude matching subproblem. Thus, trajectory-based techniques provide a basis for an approach equivalent to traveltime tomography.

Trajectory-based methods, also known as ray-based methods, have been proposed for both modelling electromagnetic wave propagation and imaging. The earliest treatments focused on the higher frequency end of the spectrum, occupied by optical and radar waves (Kline & Kay 1965; Luneburg 1966; Choudhary & Felsen 1973; Keller & Lewis 1995). The primary applications in geophysics have been to ground-penetrating radar (Lager & Lytle 1977; Daily & Lytle 1983; Davis & Annan 1989; Olsson *et al.* 1992; Goodman 1994; Vasco *et al.* 1997; Peterson 2001; Huisman *et al.* 2003). More recently, trajectory-based methods have been developed for lower frequency diffusive electromagnetic propagation and imaging (Lee & Xie 1993; Nekut 1994; Virieux *et al.* 1994; Yu & Edwards 1997; Lee *et al.* 2002). I should also point out early work by Cohen & Lewis (1967) on ray methods for the diffusion equation. In these previous formulations, either the term associated with displacements currents or the term associated with conduction currents is assumed to be negligible. Such assumptions are invalid for intermediate frequencies and when modelling broad-band electromagnetic wave propagation one must consider all terms in the governing equations.

In this paper I derive a time-domain asymptotic expression describing the evolution of a broad-band electromagnetic wavefield. The expression is valid for propagation in a smoothly varying 3-D heterogeneous earth model. By smoothly varying, I mean that the length scale of the heterogeneity is greater than the length scale associated with the spatial variation in the electromagnetic field as it propagates (Anile *et al.* 1993). Note that this does not preclude the existence of sharp interfaces in the background model. Such interfaces must be included as boundary conditions in the formulation, as is done in ray-based modelling of elastic wave propagation (Aki & Richards 2002). The smoothness assumption is compatible with the goal of updating an Earth model in order to solve the inverse problem. A finite collection of observations can typically only resolve smoothly varying heterogeneity. Thus, the method is useful in predicting wavefields and computing sensitivities as a means of solving the inverse problem. For smoothly varying media, the method is applicable over a broad range of frequencies and is capable of modelling diffusive as well as hyperbolic propagation. However, the methods fail at low frequencies, of the order of a few hertz or less, as the governing equation becomes effectively elliptic and the concept of propagation is no longer meaningful.

2 METHODOLOGY

In this section I consider the equations governing the evolution of the electric field when both displacement and conduction currents are important. By considering the method of multiple-scales, which is based upon the difference between the length-scale of field variations across a propagating electromagnetic front and the length-scale of the heterogeneity, I derive an asymptotic expression for the electric field. The high- and low-frequency limits of the asymptotic solution describe hyperbolic (delta-like) and parabolic (diffusive) behaviour, respectively.

2.1 Governing equation

The governing equations are Maxwell's equations in the presence of a current source $\mathbf{J}^s$

$$\nabla \times \mathbf{E} = -\frac{\partial \mathbf{B}}{\partial t} \tag{1a}$$

$$\nabla \times \mathbf{H} = \frac{\partial \mathbf{D}}{\partial t} + \mathbf{J}^c + \mathbf{J}^s \tag{ab}$$

where $\mathbf{E}(\mathbf{x}, t)$ is the electric field intensity, $\mathbf{B}(\mathbf{x}, t)$ is the magnetic flux density, $\mathbf{H}(\mathbf{x}, t)$ is the magnetic field intensity, $\mathbf{D}(\mathbf{x}, t)$ is the electric displacement, $\mathbf{J}^c$ $(\mathbf{x}, t)$ is the conduction current. The conduction current $\mathbf{J}^c(\mathbf{x}, t)$ is related to the electric field by Ohm's law

$$\mathbf{J}^c(\mathbf{x}, t) = \sigma(\mathbf{x})\mathbf{E}(\mathbf{x}, t). \tag{2}$$

The constitutive relations

$$\mathbf{B}(\mathbf{x}, t) = \mu(\mathbf{x})\mathbf{H}(\mathbf{x}, t) \tag{3}$$

$$\mathbf{D}(\mathbf{x}, t) = \varepsilon(\mathbf{x})\mathbf{E}(\mathbf{x}, t) \tag{4}$$

may be substituted into eqs (1a) and (1b), resulting in

$$\nabla \times \mathbf{E} = -\mu \frac{\partial \mathbf{H}}{\partial t} \tag{5a}$$

$$\nabla \times \mathbf{H} = \varepsilon \frac{\partial \mathbf{E}}{\partial t} + \sigma \mathbf{E} + \mathbf{J}^s. \tag{5b}$$

Taking the time derivative of (5b) gives

$$\nabla \times \frac{\partial \mathbf{H}}{\partial t} = \varepsilon \frac{\partial^2 \mathbf{E}}{\partial t^2} + \sigma \frac{\partial \mathbf{E}}{\partial t} + \frac{\partial \mathbf{J}^s}{\partial t}. \tag{6}$$

In the derivation of the asymptotic expression I shall neglect the current source term in eq. (6). The term $\partial \mathbf{J}^s / \partial t$ will be included in the construction of the electromagnetic field at the final stage, as a source function. Solving eq. (5a) for the time derivative of $\mathbf{H}(\mathbf{x}, t)$ and substituting it into eq. (6) gives an equation for $\mathbf{E}(\mathbf{x}, t)$

$$\nabla \times \mu^{-1} \nabla \times \mathbf{E} + \varepsilon \frac{\partial^2 \mathbf{E}}{\partial t^2} + \sigma \frac{\partial \mathbf{E}}{\partial t} = 0. \tag{7}$$

I emphasize that the coefficients $\sigma(\mathbf{x})$, and $\varepsilon(\mathbf{x})$ may vary as a function of position.

2.2 The method of multiple scales

Eq. (7) is a vector differential equation with variable coefficients which is typically solved numerically (Alumbaugh *et al.* 1996). However, numerical approaches are usually computationally intensive and it is worth developing useful approximations. This is particularly true when one wishes to solve the inverse problem of finding

the variable coefficients, such as determining $\sigma(\mathbf{x})$, given observations of $\mathbf{E}(\mathbf{x}, t)$.

In this paper I adopt the method of multiple scales, also known as the two-timing method or the averaged Lagrangian technique (Gardner & Morikawa 1960; Whitham 1974). This approach is related to the so-called high-frequency method (Courant & Hilbert 1962; Kline & Kay 1965; Lewis 1965; Luneburg 1966) but is somewhat more general. In particular, using the method of multiple scales one is able to treat dispersive and diffusive waves (Anile *et al.* 1993; Korsunsky 1997). To my knowledge, the method of multiple scales has not been used in the study of electromagnetic wave propagation within the Earth. Perhaps this is due to the ease of working with asymptotic expansions which are based upon frequency ω. If one is simply interested in developing solutions that model wave-like (hyperbolic) propagation, the most direct approach involves an expansion in inverse powers or inverse fractional powers of ω (Kline and Kay 1965). Similar considerations hold when one is only interested in studying diffusive propagation (Virieux *et al.* 1994). However, one must then neglect the term representing displacement currents in the governing equation before introducing the asymptotic series solution in inverse powers of $\sqrt{\omega}$ (Virieux *et al.* 1994). It was not until relatively recently (Stewart *et al.* 1994; Frangos *et al.* 2004) that experimental systems were developed which could operate in an intermediate frequency range where both conduction and displacement currents are important. In this regime, an expansion in inverse powers of ω emphasizes the high-frequency behaviour and the effect of displacement currents and does not capture phenomena due to conduction currents. Because of this limitation, I chose to use the method of multiple scales instead of an expansion in inverse powers of ω. As shown below, the method of multiple scales allows for the modelling of both diffusive and wave-like propagation as well as intermediate behaviour.

In what follows I will be modelling a propagating electromagnetic field generated by an active source. Initially, the background electromagnetic field is in a quiescent state. Suddenly, the source is activated and an electromagnetic disturbance propagates into the surrounding medium. The method of multiple scales begins with the notion that there are two scales of importance in the propagation of electromagnetic energy through the subsurface. Specifically, there is a spatial variation in medium properties [$\sigma(\mathbf{x})$, and $\varepsilon(\mathbf{x})$] and there is the spatial and temporal variation in the electromagnetic field as the disturbance propagates through the subsurface. The scale length associated with the propagating field is defined across the moving front and represents the transition from the initial background value to the field amplitude of the electromagnetic disturbance. Note that the scale length of the propagating front is a function of its frequency content. The underlying assumption of the method of multiple scales is that there is a separation of scales. In particular, the scale length associated with the variation in medium properties is assumed to be much larger than the scale length of the propagating electromagnetic disturbance. If I denote the scale of variation of the background properties by L and the mean length of the variation across the propagating front by l, then $L \gg l$. The ratio of scales is characterized by the parameter $\epsilon = l/L$ which, by assumption, is much smaller than 1. The method of multiple scales develops an asymptotic expansion based upon ϵ rather than one based upon ω.

In the method of multiple scales one defines slow variables $\mathbf{X}$ and T in terms of the physical variables $\mathbf{x}$ and t by

$$X^i = \epsilon x^i,$$

and

$$T = \epsilon t,$$

where ϵ was defined above as the ratio l/L. The electric field is then written as a formal power series expansion in ϵ (Anile *et al.* 1993),

$$\mathbf{E}(\mathbf{X}, \theta) = \sum_{p=0}^{\infty} \epsilon^p \mathbf{E}_p = e^{i\theta} \sum_{p=0}^{\infty} \epsilon^p \mathbf{A}_p(\mathbf{X}), \tag{8}$$

where $\theta(\mathbf{X})$, and $\mathbf{A}_p(\mathbf{X})$ are unknown functions which are to be estimated after substituting the power series (8) into the governing eqs (7). The result is an expression containing terms of various orders in the expansion parameter ϵ. By considering terms of lowest order in ϵ, which are the most important for ϵ small, I obtain equations constraining $\theta(\mathbf{X}, T)$ and $\mathbf{A}_0(\mathbf{X})$, as shown in Appendix A. It must be noted that asymptotic series may be and often are divergent (Kravtsov & Orlov 1990). That is, successive terms may not decrease in the sum as p increases. The essential point is that as $\epsilon \to 0$ the first few terms of the series dominate and provide a good approximation to $\mathbf{E}(\mathbf{X}, \theta)$.

The function $\theta(\mathbf{x})$ is the local phase which may be written in the partitioned form [eq. (A10)]

$$\theta(\mathbf{X}, T) = \omega T - \varphi(\mathbf{X}) \tag{9}$$

where ω is the temporal frequency and $\varphi(\mathbf{X})$ satisfies the eikonal equation

$$\nabla\varphi \cdot \nabla\varphi = \gamma \tag{10}$$

a non-linear partial differential equation which depends upon the electrical properties of the medium

$$\gamma = \mu\omega(\omega\varepsilon - i\sigma) \tag{11}$$

[see eq. (A19) in the appendix]. From eqs (9), (10), and (11) it is clear that $\theta(\mathbf{X})$ depends both implicitly and explicitly upon the temporal frequency ω. The functions $\mathbf{A}_p(\mathbf{X})$, $p = 1, 2, \ldots$ are successive corrections to the zeroth-order amplitude $\mathbf{A}_0(\mathbf{X})$.

Locally, expression (8) is in the form of a propagating disturbance or front. For $\epsilon \ll 1$, the terms in the series decrease rapidly with increasing p. Typically, only the first one or two terms are sufficient to describe the wavefield. The general approach involves substituting the series (8) into the governing eq. (7). The result is an expression containing terms of various orders in ϵ. By considering terms of zeroth-order in ϵ, I derive an equation governing the distribution of the local phase $\theta(\mathbf{x})$. The first-order terms give rise to a transport equation describing the evolution of the amplitude. The details of this procedure are to be found in the appendix of this paper.

One characteristic of the asymptotic approach is that the solutions are defined along trajectories or ray paths through the earth model (Keller & Lewis 1995). These paths are denoted by the vector $\mathbf{s}(s)$ which is a function of s, a parameter describing the position along the trajectory. The trajectory $\mathbf{s}(s)$ is the solution of the ray equations

$$\frac{d\mathbf{s}}{ds} = \frac{1}{\sqrt{\gamma}}\mathbf{p} \tag{12a}$$

$$\frac{d\mathbf{p}}{ds} = \nabla\sqrt{\gamma} \tag{12b}$$

where

$$\mathbf{p} = \nabla\varphi$$

and as shown in the appendix [eqs (A20) and (A11)]. In ray coordinates, defined by the trajectory $\mathbf{s}(s)$, φ may be written as a

© 2007 The Author, *GJI*, **168,** 949–963
Journal compilation © 2007 RAS

path-integral

$$\varphi(\mathbf{s}_f) = \int_{s_0}^{s_f} \sqrt{\gamma} ds \tag{13}$$

where the path of integration is along the ray **s** extending from the initial point s_0 to the final point s_f. In most applications one is interested in defining the trajectory between a source and receiver point, so-called two-point ray tracing (Keller 1968). I employ a shooting method coupled to a globally convergent Newton–Raphson routine, as described in Press *et al.* (1992, p. 749). In essence, a trial initial value of **p** is adopted and a fourth order Runge–Kutta technique with adaptive step-size control (Gear 1971) is used to trace the trajectory. A misfit function, which measures the discrepancy between the final point of the trajectory and the desired final point, is minimized. The Newton–Raphson routine is used to update the vector **p** at s_0 such that the end point of the trajectory moves towards the desired point, minimizing the misfit function. Because the total trajectory length is unknown *a priori*, I must solve for the final value of s as well as for **s** and **p**, a form known as a free boundary problem (Press *et al.* 1992, p. 748).

As shown in Appendix A, the zeroth-order amplitude satisfies a linear vector transport equation. Along the trajectory, **s**(s), one may derive a scalar differential equation for the squared magnitude of $\mathbf{E}_0$ [eq. (A28)]

$$\frac{dE_0{}^2}{ds} + \Psi(s) E_0{}^2 = 0, \tag{14}$$

where

$$\Psi(s) = \nabla \cdot \mathbf{p} + \mu\omega\sigma + 2\mu\omega^2\varepsilon i. \tag{15}$$

Eq. (14) may be integrated explicitly, resulting in an expression

$$E_0{}^2(s) = E_0{}^2(s_0) \exp\left\{ - \int_{s_0}^{s} \Psi(s)\, ds \right\} \tag{16}$$

in terms of the initial field $E_0(s_0)$ at the source point s_0, the medium properties, and phase gradient vector **p**. Note that the wavefield decay with distance along the trajectory is controlled by $\Psi(s)$. The various terms in $\Psi(s)$ may be interpreted physically. The term $\nabla \cdot \mathbf{p}$ describes the decay due to the divergence of the trajectories. The term $\mu\omega\sigma$ describes decay due to attenuation related to the conductivity of the medium. The imaginary term $\mu\omega^2\varepsilon i$ induces an oscillatory behaviour in the amplitude decay with distance.

Eq. (16) describes the evolution of the amplitude of the electric field with distance away from the source. However, the electric field is a vector quantity and to complete the specification I need to compute the evolution of the vector components. Computing the vector components is described in some detail in Kline & Kay (1965, p. 167) and Kravtsov & Orlov (1990, p. 230). The integration of the vector components is best done in ray coordinates, specified by the trajectory **s**(s). It may be shown that the electric and magnetic field vectors are orthogonal to phase gradient vector **p** (Kravtsov & Orlov 1990, p. 228). Following Kline & Kay (1965, p. 167), one can derive an equation describing the evolution of a unit vector in the direction of the electric field, denoted by $\hat{\mathbf{E}}(s)$, along the trajectory

$$\hat{\mathbf{E}}_0' + (\hat{\mathbf{E}}_0 \cdot \mathbf{s}'')\mathbf{s}' = 0 \tag{17}$$

where the primes indicate differentiation with respect to the variable s.

2.3 Constructing the Zeroth-Order Electromagnetic Field

Eq. (8) provides a representation of the electromagnetic field as a propagating wave. In this subsection I outline the construction of a zeroth-order approximation to the electromagnetic field. The derivation implicitly assumes a propagating disturbance at a single frequency. A general field may be constructed by linear superposition over a range of frequencies. To model the propagation effects I utilize the zeroth-order term of the series (8). Incorporating the form (9) for θ, I write $\mathbf{E}_0$ as

$$\mathbf{E}_0(\mathbf{s}_f, T) = e^{i\omega T} e^{-i\varphi} \mathbf{A}_0(\mathbf{s}_f), \tag{18}$$

where $\varphi(\mathbf{s}_f)$ is given by the integral (13) and $\mathbf{A}_0(s)$ is given by $e^{i\theta} E_0(s) \hat{\mathbf{E}}_0(s)$ where $E_0^2(s)$ is the solution of the transport eq. (16) and $\hat{\mathbf{E}}_0$ is obtained by solving eq. (17). I can factor $\sqrt{\omega}$ out of the integrand in (13) and write the integral as

$$\varphi(\mathbf{s}_f) = \sqrt{\omega} \int_{s_0}^{s_f} \sqrt{\omega\mu\varepsilon - i\mu\sigma}\, ds. \tag{19}$$

For a general source the amplitude of the various frequency components will vary. In order to model this variation I include a weighting function $\Pi(\omega)$ as part of a total amplitude function $\mathbf{U}(\mathbf{s}_f, \omega)$

$$\mathbf{U}(\mathbf{s}_f, \omega) = \Pi(\omega) \mathbf{A}_0(\mathbf{s}_f). \tag{20}$$

Writing the superposition as an integral over ω produces the expression

$$\mathbf{E}_0(\mathbf{s}_f, T) = \int_{-\infty}^{\infty} \mathbf{U}(\mathbf{s}_f, \omega) e^{-i\varphi} e^{i\omega T}\, d\omega \tag{21}$$

for the electromagnetic field as a function of space and time. Because the integral over ω is in the form of an inverse Fourier transform I may write the total field as

$$\mathbf{E}_0(\mathbf{s}_f, T) = \mathcal{F}^{-1}\{e^{-i\varphi}\} * \mathbf{u}(\mathbf{s}_f, T) \tag{22}$$

where $\mathcal{F}^{-1}$ denotes the inverse Fourier transform, $*$ denotes a temporal convolution, and $\mathbf{u}(\mathbf{s}_f, T)$ is the inverse Fourier transform of $\mathbf{U}(\mathbf{s}_f, \omega)$. In general, the inverse Fourier transform of the first factor on the right-hand side of eq. (22) cannot be evaluated explicitly. However, some physical insight is afforded by considering two commonly encountered situations: when $\omega\varepsilon \gg \sigma$ (wave-like regime) or when $\omega\varepsilon \ll \sigma$ (diffusive regime).

2.3.1 'Wave-like' regime

When the term $\omega\varepsilon$ dominates σ in the integrand of (19), $\varphi(\mathbf{s}_f)$ is adequately approximated by

$$\varphi(\mathbf{s}_f) = \omega \int_{s_0}^{s_f} \sqrt{\mu\varepsilon}\, ds. \tag{23}$$

If I define the integral

$$\Upsilon(\mathbf{s}_f) = \int_{s_0}^{s_f} \sqrt{\mu\varepsilon}\, ds \tag{24}$$

then I can write eq. (22) as

$$\mathbf{E}_0(\mathbf{s}_f, T) = \mathcal{F}^{-1}\{e^{-i\omega\Upsilon(\mathbf{s}_f)}\} * \mathbf{u}(\mathbf{s}_f, T). \tag{25}$$

The inverse Fourier transform of $e^{-i\omega\Upsilon(\mathbf{s}_f)}$ is a delta function shifted by $\Upsilon(\mathbf{s}_f)$. Thus, the time-domain expression for $\mathbf{E}(\mathbf{s}_f, T)$ is simply

$$\mathbf{E}_0(\mathbf{s}_f, T) = \mathbf{u}(\mathbf{s}_f, T - \Upsilon(\mathbf{s}_f)), \tag{26}$$

the calculated amplitude shifted by $\Upsilon(\mathbf{s}_f)$. The time-domain expression (26) and the traveltime (24) are identical to the high-frequency

asymptotic solutions derived in previous studies using power series expansions in ω^{-1} (Luneburg 1966; Kline & Kay 1965; Keller & Lewis 1995). These expressions are useful in modelling ground-penetrating radar wave propagation within the Earth (Olsson *et al.* 1992; Goodman 1994; Vasco *et al.* 1997; Peterson 2001).

2.3.2 *'Diffusive' regime*

When the term $\omega\varepsilon$ is much smaller than σ the integral

$$\varphi(\mathbf{s}_f) = \sqrt{-i\omega}\int_{s_0}^{s_f}\sqrt{\mu\sigma}\,ds \tag{27}$$

is a good approximation to (19). Defining the integral

$$\tau(\mathbf{s}_f) = \int_{s_0}^{s_f}\sqrt{\mu\sigma}\,ds, \tag{28}$$

I may write eq. (22) as

$$\mathbf{E}_0(\mathbf{s}, T) = \mathcal{F}^{-1}\{e^{-\sqrt{i\omega}\tau(\mathbf{s})}\} * \mathbf{u}(\mathbf{s}, T). \tag{29}$$

Note that $\tau(\mathbf{s})$, as defined in eq. (28) represents the slowness, the inverse of the velocity, in the ray methods proposed by Lee & Xie (1993), Nekut (1994), Virieux *et al.* (1994), Yu & Edwards (1997) and Lee *et al.* (2002). Similarly, the square root frequency dependence utilized by Virieux *et al.* (1994), based upon earlier work by Tikhonov (1965), follows from the asymptotic expression (27). The time-domain expression (29) is the temporal convolution of an exponentially decaying term and the inverse Fourier transform of the amplitude term,

$$\mathbf{E}_0(\mathbf{s}, T) = \frac{\tau(\mathbf{s})}{2\sqrt{\pi T^3}}e^{-\tau^2(\mathbf{s})/4T}\,\Sigma(T) * \mathbf{u}(\mathbf{s}, T) \tag{30}$$

where $\Sigma(T)$ is a step function with the jump at the origin. This form of the zeroth-order solution was noted by Virieux *et al.* (1994) for diffusive electromagnetic wavefields. These authors also point out a physical interpretation of τ as the square root of the time associated with the arrival of the peak of the pulse (30) for a delta function source. Alternatively, for a step-function source, τ represents the time associated with the arrival of the peak of the time derivative of the waveform (Vasco *et al.* 2000).

For a general medium and intermediate frequencies one must work with the full integral (19). It is straightforward to evaluate the integral numerically. However, computing the trajectories and amplitudes requires complex ray tracing. As illustrated below, complex ray tracing is a direct extension of real ray tracing and complex rays may be computed for an arbitrary heterogeneous medium (Egorchenkov & Kravtsov 2001; Amodei *et al.* 2006).

2.4 Propagation across a discontinuity

I stated in the introduction that interfaces or discontinuities in electrical properties may be included as boundary conditions. The overall approach involves constructing asymptotic, trajectory-based solutions within the smoothly varying regions separated by the interface. The asymptotic solutions are linked by the boundary conditions placed on the field at the interface. For example, one can invoke the continuity of $\hat{\mathbf{n}} \times \mathbf{E}_0$ and $\hat{\mathbf{n}} \times \mathbf{H}_0$ across an interface, where $\hat{\mathbf{n}}$ is the normal to the surface at the point in question. This approach is similar to methods employed in the reflection and transmission of seismic waves across a boundary (Hearn & Krebes 1990; Aki & Richards 2002).

In practice, the incorporation of a discontinuity is straightforward. For example, the ray eqs (12a) and (12b) are solved numerically using the shooting method coupled to a Newton–Raphson routine, as noted above. The method is modified at the interface, where the incident electric field generates reflected and transmitted fields. The conditions for continuity across the interface results in conditions on the angles at which the reflected and transmitted trajectories leave the interface (Kline & Kay 1965, p. 174). It is not my intent to provide detailed derivations of these equations here, as propagation across discontinuities is not the focus of this paper. Furthermore, the overall procedure has been described elsewhere (Kline & Kay 1965; Kravtsov & Orlov 1990). Rather, I merely want to show how to modify the algorithm for computing the trajectory-based solution in order to account for interfaces.

By invoking continuity of the incident, reflected, and transmitted fields one arrives at conditions on the corresponding phase gradient vectors associated with each field, $\mathbf{p}^i$, $\mathbf{p}^r$, and $\mathbf{p}^t$, respectively. The conditions are (Kline & Kay 1965, p. 174)

$$\mathbf{p}^r \times \hat{\mathbf{n}} = \mathbf{p}^i \times \hat{\mathbf{n}} \tag{31}$$

and

$$\mathbf{p}^t \times \hat{\mathbf{n}} = \mathbf{p}^i \times \hat{\mathbf{n}} \tag{32}$$

where $\hat{\mathbf{n}}$ is the normal to the surface at the point in question. By a property of the vector product and using the fact that $|\mathbf{p}^i| = |\mathbf{p}^r| = \sqrt{\gamma_1}$ and $|\mathbf{p}^t| = \sqrt{\gamma_2}$, I find that

$$\sin\theta^r = \sin\theta^i \tag{33}$$

and

$$\sqrt{\gamma_2}\sin\theta^t = \sqrt{\gamma_1}\sin\theta^i \tag{34}$$

where θ^i is the angle of incidence, the angle that $\mathbf{p}^i$ makes with the normal to the surface $\hat{\mathbf{n}}$, and similarly for θ^r and θ^t. In order to compute the trajectory I use the two-point ray tracing routine mentioned above, with a modification to account for the discontinuity. That is, the ray is traced through the upper-most medium as before. However, when the interface is encountered I use eq. (34) along with the value of θ^i and the properties above (γ_1) and below (γ_2) the discontinuity to refract the trajectory as it crosses the boundary. That is, to compute the angle, θ^t, at which the transmitted field trajectory leaves the discontinuity. The ray tracing proceeds in the second medium using the Runge–Kutta technique and the new angle θ^t. The procedure continues across all relevant interfaces until the layer containing the receiver is reached. The Newton–Raphson routine is used to adjust the initial take-off angle until the receiver is reached. Thus, the original ray tracing routine is used with a finite number of adjustments, one at each discontinuity.

Once the ray is found, the amplitude is calculated by solving the transport equation and accounting for the continuity of the normal component of $\mathbf{E}$ across an interface. For example, the continuity of the electric field across the interface leads to the equation

$$(\mathbf{E}^i + \mathbf{E}^r) \times \hat{\mathbf{n}} = \mathbf{E}^t \times \hat{\mathbf{n}} \tag{35}$$

(Kline & Kay 1965, p. 176). This equation, coupled with relationships between $\mathbf{p}^i$, $\mathbf{p}^r$, $\mathbf{p}^t$, $\mathbf{E}^i$, $\mathbf{E}^r$, $\mathbf{E}^t$, $\mathbf{H}^i$, $\mathbf{H}^r$, $\mathbf{H}^t$, and the properties on each side of the interface lead to reflection and transmission coefficients associated with the discontinuity (Kline & Kay 1965, p. 178). The reflection and transmission coefficients are used to modify the field amplitudes as the waves encounter the interface. That is, they are multiplication factors which are applied to the incident field amplitude in order to calculate the transmitted and reflected field amplitudes.

In summary, the presence of a discontinuity does not fundamentally alter the process of computing the trajectory associated with a broad-band electromagnetic wave. I still employ the Newton–Raphson routine to conduct two-point ray tracing. The discontinuity induces a refraction of the ray as it crosses the interface. This refraction is computed using (34) and incorporated into the Runge–Kutta routine for computing the trajectory. Similarly, a trajectory associated with the reflected wave may be calculated using eq. (33) and the two-point ray tracing routine. The amplitudes are still determined by solving the transport equation in the regions separated by the interface. The discontinuity itself gives rise to a partitioning of energy which is described by reflection and transmission coefficients. The computation of reflection and transmission coefficients is straightforward and has been discussed elsewhere (Kline & Kay 1965; Kravtsov & Orlov 1990; Borovikov & Kinber 1994). Because the main focus of this paper is the propagation of broad-band electromagnetic wavefields in smoothly varying media, I shall not discuss the computation of reflection and transmission coefficients any further.

2.5 Validity of the Trajectory-Based Representation

I conclude the Methodology section with some observations concerning the validity of the trajectory-based solution. Because the expansion parameter of the asymptotic series (8) is $\epsilon = l/L$, the ratio of the length-scale of the electromagnetic variation to the length-scale of the heterogeneity, the domain of validity is somewhat different then for an asymptotic solution in frequency, ω. For example, the solution presented here is valid for both diffusive and wave-like propagation, as is evident from the end-member solutions (30) and (26), respectively. In that sense, the solution connects ray methods used to model high-frequency propagation, such as ground penetrating radar (Olsson *et al.* 1992; Goodman 1994; Vasco *et al.* 1997; Peterson 2001), and low-frequency ray methods (Lee & Xie 1993; Nekut 1994; Virieux *et al.* 1994; Yu & Edwards 1997; Lee *et al.* 2002). Thus, under appropriate circumstances, the approach allows one to model electromagnetic propagation in the Earth at intermediate frequencies,

The factor determining the convergence of the power series (8) is the ratio of the length-scale of the electromagnetic variation, l, to the length-scale of the heterogeneity, L. The length-scale of the wavefield variation is a frequency-dependent property, given by

$$l = \frac{2\pi v}{\omega} \tag{36}$$

where v is the velocity of the disturbance and ω is the frequency of interest. Thus, the ratio l/L is given by

$$l/L = \frac{2\pi v}{\omega L}$$

and the series converges when

$$L \gg \frac{2\pi v}{\omega}. \tag{37}$$

For a given frequency and a given velocity v it is straightforward to determine the length-scale of heterogeneity for which the series converges. For example, in shallow soils the heterogeneity should have a scale length greater then 0.5 m for a 200 MHz ground penetrating radar system, as described in the Applications section below. Given values of v, ω, and L one can estimate the parameter ϵ and compute the relative magnitude of the successive terms in the power series (8). The criterion (37) is compatible with the constraints on solving the inverse problem. That is, one is typically trying to determine smoothly varying heterogeneity. In most cases it is not possible to resolve rapidly varying features using data gathered at some distance from the object of interest.

3 APPLICATIONS

In this section I consider both a set of numerical illustrations of the computation of trajectory-based solutions as well as two field applications. The first field application involves broad-band downhole data from an experiment in Richmond, California. The second field experiment employed ground penetrating radar to image heterogeneity between two boreholes at the Boise Hydrogeophysical Research Site in Idaho.

3.1 Numerical illustrations

The numerical examples are intended to illustrate the trajectory-based computation and to compare calculated amplitudes with an analytic whole-space solution for a magnetic dipole source. The first task in constructing a trajectory-based solution is solving the set of differential eqs (12a) and (12b) for the trajectory **s** and slowness vector **p** as functions of s, a parameter signifying the distance along the path. Because the quantity γ is generally complex, the equations (12a) define a complex trajectory and both **s** and **p** are complex vectors. This fact does not pose any fundamental difficulty and complex trajectories have been described previously (Seckler & Keller 1959; Felsen 1976; Kravtsov *et al.* 1999; Egorchenkov & Kravtsov 2001; Amodei *et al.* 2006). The procedure for defining a complex trajectory is identical to that used in the real case, I simply solve the equations for the real and imaginary components.

3.1.1 A Homogeneous Whole-Space

In the first illustration I compute waveforms for a broad-band transmitter situated in a homogeneous whole-space with a conductivity of 0.05 S m^{-1} and a dielectric permittivity of 9.0×10^{-11} F m^{-1}. The receiver is offset along a 45° line from the vertical magnetic dipole source. After the trajectory is computed I calculate the amplitude using (16), which is an integral along the path **s**(s). It may be shown that the divergence of **p** in the integral expression (16) is related to the divergence of the trajectories with distance from the source (Kravtsov & Orlov 1990, p. 13). Thus, to compute the divergence I simply trace a set of trajectories by perturbing the take-off angles, as shown schematically in Fig. 1. In three-dimensions three rays are needed to calculate the divergence associated with the central ray. Given the phase and amplitude I can use eq. (18) to obtain the complex electric field at the receiver for a given frequency ω. A source with any particular frequency dependence may be included in the total amplitude function $\mathbf{U}_0(\mathbf{s}, \omega)$ [eq. (20)]. For the calculations at hand I use a vertical magnetic dipole source as described in Alumbaugh & Morrison (1995) and Spies & Habashy (1995). In this case the transmitter is an infinitesimal solenoid carrying current I with n_T turns, and an area a_T with axis $\mathbf{u}_T$. The current source vector $\mathbf{J}^s$ for a solenoid located at $\mathbf{x}_T$ is

$$\mathbf{J}^s(\mathbf{x}) = n_T I a_t \nabla \times \mathbf{u}_T \delta(\mathbf{x} - \mathbf{x}_T) \tag{38}$$

(Spies & Habashy 1995). The resulting field at a receiver located at $\mathbf{x}_r$ is given by the integral

$$\mathbf{E}(\mathbf{x}_r) = \int_v \mathbf{G}(\mathbf{x}_r, \mathbf{x}) \cdot \mathbf{J}^s(\mathbf{x}) d\mathbf{x} \tag{39}$$

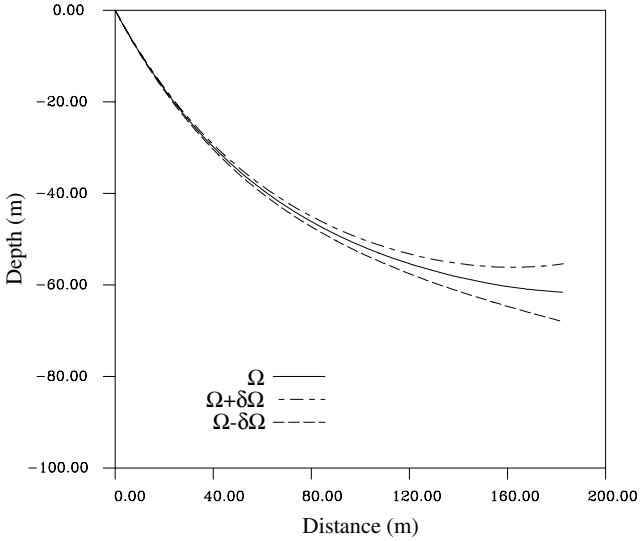

Figure 1. 2-D illustration of the method used to quantify trajectory divergence for computing amplitudes. Given a base trajectory, denoted by Ω, two adjacent trajectories are calculated by perturbations about the base take-off angle. The divergence is estimated from the spreading of the trajectories. For a 3-D calculation three rays must be traced.

where ν is the source volume and $\mathbf{G}(\mathbf{x}_r, \mathbf{x})$ is the Green's function which is given by eq. (22) for a point source.

Using a whole-space model allows me to compare the trajectory-based results with the analytic expressions of Alumbaugh & Morrison (1995) and Spies & Habashy (1995). In (Figs 2 and 3) I compare the trajectory-based amplitude variations as a function of distance with those computed using the analytic expression of Spies & Habashy (1995). The comparisons are for a three decade variation in frequency between 0.1 and 100.0 MHz. Overall, the agreement is quite good over the entire frequency band and distance range.

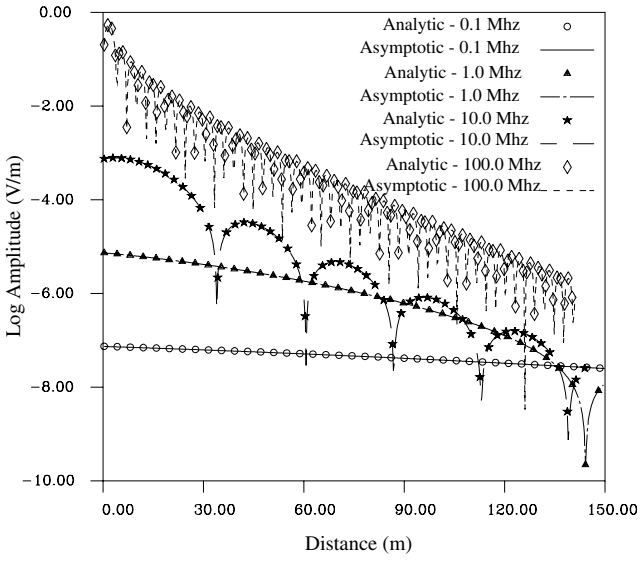

Figure 2. Real component of the field amplitude as a function of distance from the source. The symbols denote quantities computed using the analytic expression of Spies & Habashy (1995) while the curves represent trajectory-based estimates made using the techniques described in this paper. The amplitudes are computed at four difference frequencies spanning three decades.

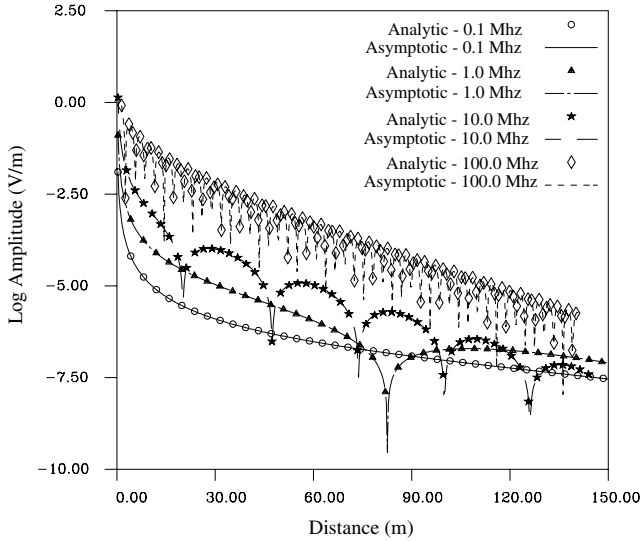

Figure 3. Imaginary component of the field amplitude as a function of distance from the source. The symbols denote quantities computed using the analytic expression of Spies & Habashy (1995) while the curves represent trajectory-based estimates.

3.1.2 A vertically-varying model

In the second example the conductivity varies in a quadratic fashion, decreasing with depth, while the dielectric permittivity is a constant 9.0×10^{-11} F m^{-1} (Fig. 4). I used the Newton–Raphson routine to compute trajectories through the structure shown in Fig. 4. In Fig. 5 the real components of five trajectories are shown for take-off angles (angles are defined from the horizontal axis) varying between 15° and 55°. The trajectories are computed for a frequency of 0.1 MHz and the source point is located at the origin. The trajectories curve due to the vertical decrease in conductivity which dominates at this frequency. I also examine how the trajectories vary with frequency, as shown in Fig. 6. In this case the take-off angle is held fixed, at 55°, while the frequency ranges from 0.1 MHz to 100.0 MHz. At the lower frequencies, below about 10.0 MHz the rays bend in response to the conductivity variation. As the frequency increases

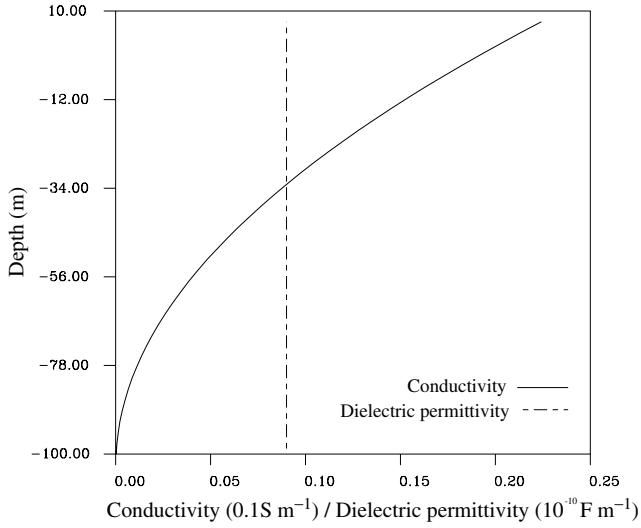

Figure 4. Vertical variation in conductivity, $\sigma(\mathbf{x})$, and dielectric permittivity, $\varepsilon(\mathbf{x})$, for the model used to compute trajectories for the numerical illustration.

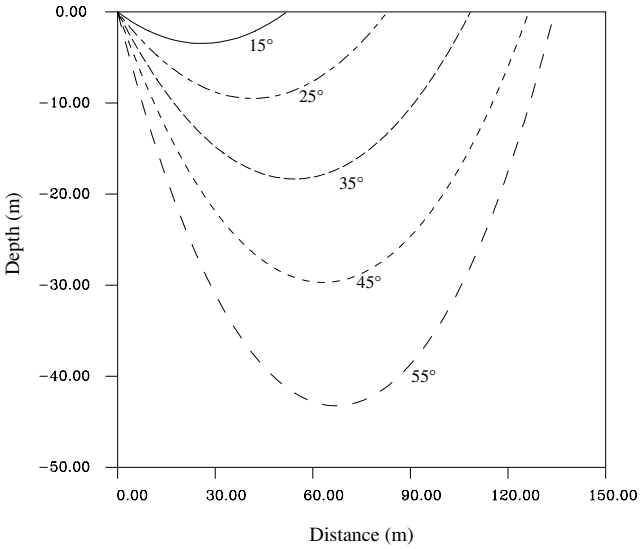

Figure 5. Five trajectories, each corresponding to a different take-off angle. The take-off angle is angle at which the trajectory leaves the source point, measured from the horizontal axis.

beyond 10.0 MHz the curvature of the trajectories decreases until the path becomes a straight line at around 100.0 MHz. Thus, at the higher frequencies the propagation is dominantly influenced by the dielectric permittivity which is constant. This follows from the fact that $\gamma = \sqrt{\omega^2\mu\varepsilon - i\mu\omega\sigma}$ controls the phase distribution via the eikonal equation. For ω large enough, the constant $\omega^2\mu\varepsilon$ dominates, and γ is essentially constant. Trajectories in a medium with constant γ are straight lines. In tandem with the changes in the geometry of the trajectories, we also observe the appearance of a significant imaginary component at around 10.0 MHz (Fig. 6).

3.1.3 A heterogeneous model

As a test of the algorithm in the presence of lateral heterogeneity, I computed trajectories for the conductivity model shown in Fig. 7.

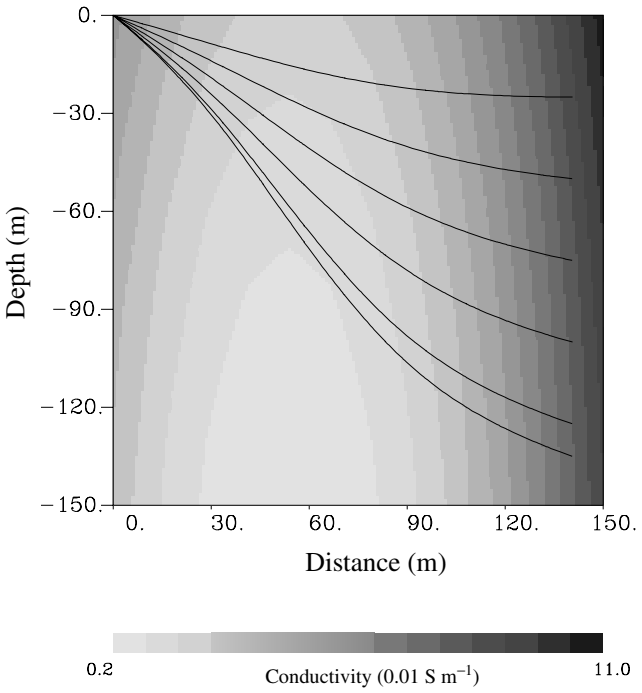

Figure 7. 2-D, heterogeneous conductivity model used to compute trajectories associated with a 75 MHz electric field component. The trajectories are denoted by solid lines in this figure. The grey scale indicates the variation in conductivity with darker shades indicating higher conductivity.

The frequency used in this illustration was 75 MHz. As in the previous example, the dielectric permittivity is a constant 9.0×10^{-11} F m^{-1}. The model contains a resistive body at depth, just to the left of the centre of the figure. Rays are traced to six points at various depths (25, 50, 75, 100, 125, and 135 m) but at the same offset from the source, 140.6 m. The conductivity varies by over an order of magnitude from 0.002 to 0.11 S m^{-1}. All the rays bend in response to the spatial variations in conductivity. The degree of bending is evident in Fig. 8, which compares the ray path for the heterogeneous

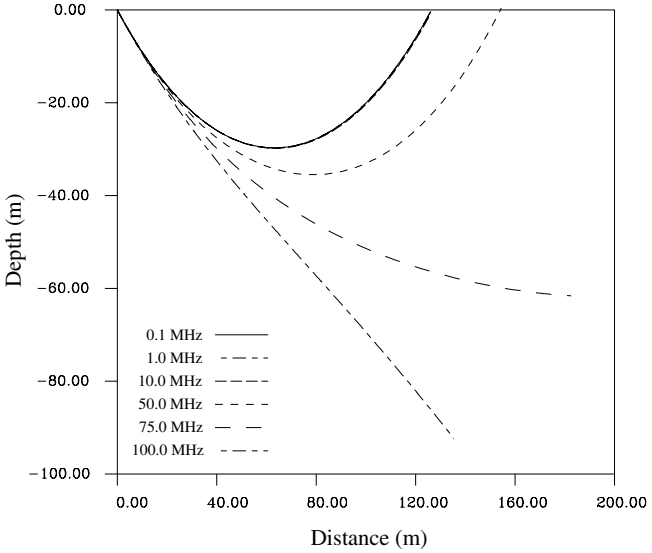

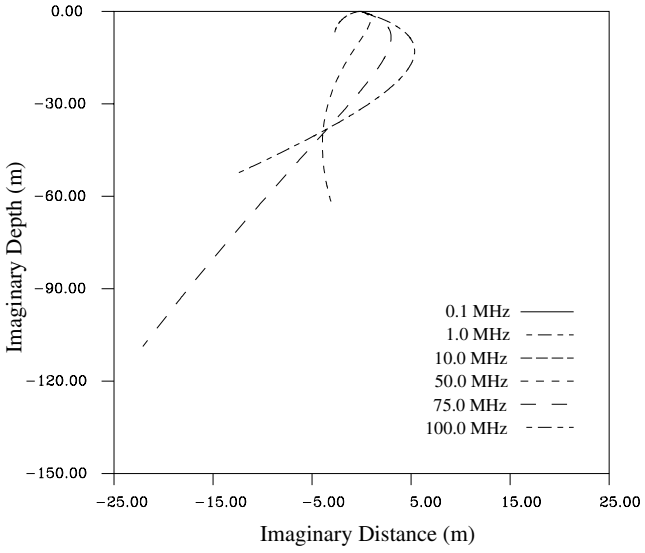

Figure 6. Real (left panel) and imaginary (right panel) components of six different trajectories. Each trajectory corresponds to a different frequency, as indicated by the legend. All of the trajectories leave the source at the same take-off angle, 55°. Real trajectories corresponding to 0.1, 1.0 and 10.0 Mhz overlap because the ray paths are essentially identical for this frequency range. At frequencies of 0.1 and 1.0 Mhz the imaginary trajectories have lengths close to zero.

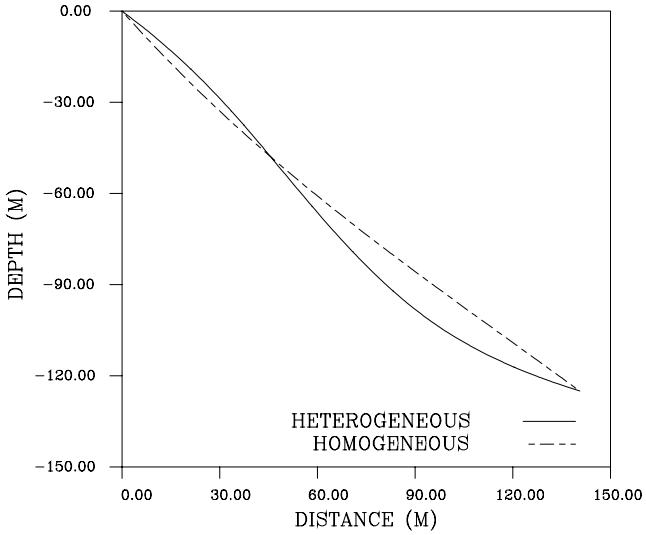

Figure 8. Comparison of a trajectory associated with a homogeneous background conductivity model and a trajectory computed in the model shown in Fig. 7. The heterogeneity causes the trajectory to bend toward the resistive region of the model and away from areas of high conductivity.

model with a ray path for a homogeneous conductivity model. The ray appears to bend towards the resistive body and away from the high conductivity regions.

3.2 Test of a wide-band downhole transmitter at the Richmond Field Station, California

As mentioned in the Introduction, there is interest in the development of a broad-band electromagnetic transmitter. A broad-band source would be useful for shallow geophysical investigations and crosswell studies (Stewart *et al.* 1994; Becker *et al.* 1999; Frangos *et al.* 2004). In an effort to construct a practical crosswell electromagnetic system, investigators at Berkeley Laboratory designed a prototype downhole transmitter which operated in the range of a few kilohertz to roughly 300 kHz (Becker *et al.* 1999). The transmitter consisted of a solenoidal ferrite core composed of six solid cylindrical pieces held together by nylon stripping (Becker *et al.* 1999). The ferrite loaded transmitter solenoid is driven by 5 A, 1.1 μS pulses which, due to a finite fall time, are broadened and take the shape shown in Fig. 9. The total system impulse response, which includes the receiver characteristics, is also shown in Fig. 9. It was obtained by putting the receiver in very close coupling with the transmitter, thereby minimizing ground production effects (Becker *et al.* 1999).

The transmitter was placed in a borehole at Berkeley Laboratories Richmond Field Station. Electrical logs for the shallow subsurface indicate that the resistivity of the unconsolidated material is about 20 ohm-m (Becker *et al.* 1999). The receiver was located 20 m above the transmitter for the test I shall consider. Data were acquired using a digital oscilloscope and 900 pulses were averaged to produce the recorded signal. The recorded waveform was sampled at a 100 nS sample rate. The raw stacked data were offset in both time and baseline voltage level and had to be empirically corrected for these offsets (Becker *et al.* 1999).

The data are modelled using the trajectory-based approach described above. Broad-band waveforms, in the frequency range of 1 kHz to 300 kHz, are computed for 128 frequencies. This is accomplished by ray tracing through a homogeneous whole-space model with a resistivity of 20 ohm-m. The trajectory-based impulse response is convolved with the source wavelet and the transmitter response, which may be obtained from the data in Fig. 9. The calculated electric field is shown in Fig. 10, denoted by the solid line. The calculated field values are in general agreement with the observed values (unfilled circles). Note that some deviation is to be expected due to the use of a homogeneous whole-space to compute the field. As noted in Frangos *et al.* (2004) there is some variation in conductivity with depth at the Richmond Field Station. Given the simplifications used in the modelling, the fit to the data appears satisfactory.

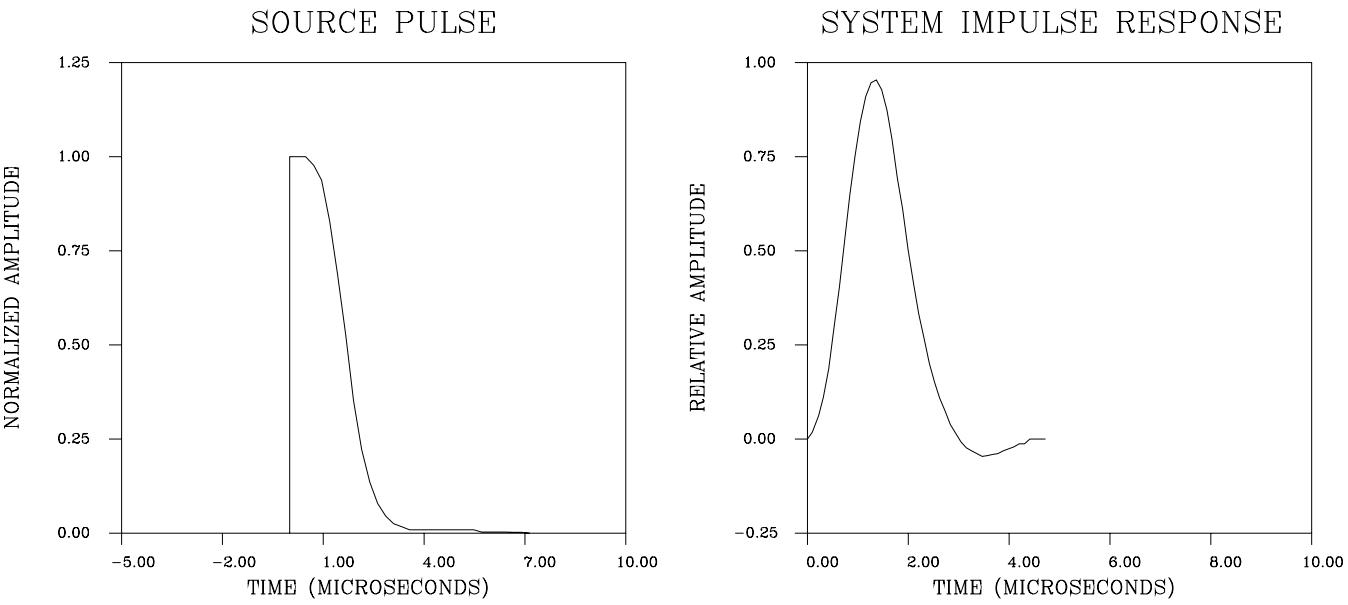

Figure 9. (Left panel) Observed source pulse output by the broad-band downhole transmitter which was tested at the Richmond Field Station. (Right panel) System impulse response for the equipment used for the downhole experiment at the Richmond Field Station.

© 2007 The Author, *GJI*, **168,** 949–963
Journal compilation © 2007 RAS

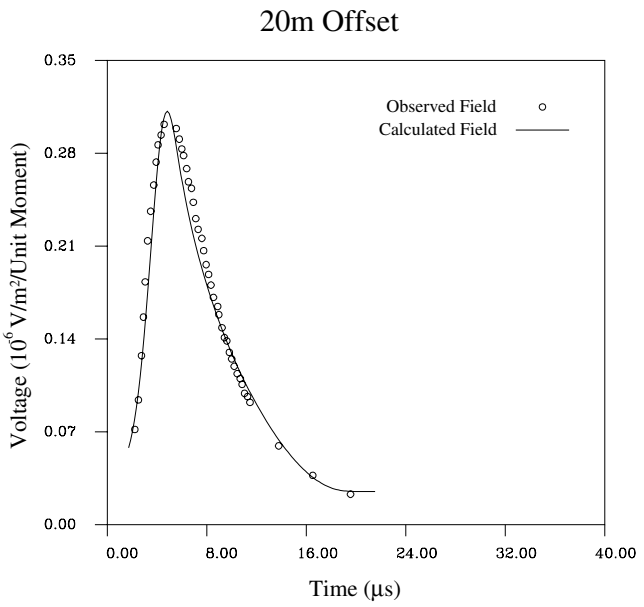

Figure 10. Observed (open circles) and calculated (solid line) electric field for the downhole experiment.

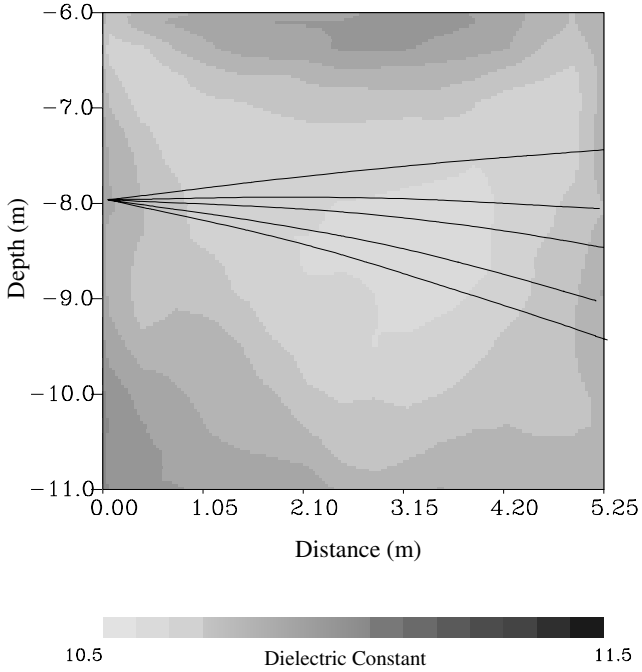

Figure 11. The grey scale in this figure depicts the spatial variation in the dielectric constant. The estimates are derived from an inversion of ground penetrating radar first arrival times. The curves through the model are trajectories associated with the propagation of radar energy from a source to five receivers situated in the borehole on the right.

3.3 Crosswell ground penetrating radar observations gathered at the Boise Hydrogeophysical Research Site

The Boise Hydrogeophysical Research Site is a field area in Boise, Idaho dedicated to the development and testing of hydrologic and geophysical methods for characterizing the flow properties of heterogeneous aquifers (Clement *et al.* 2006). The research site is underlain by a shallow alluvial aquifer comprised of unconsolidated sands, gravels, and clays. The water table is found at roughly 2.5 m below the ground surface though it fluctuates in a seasonal manner.

In the fall of 1997 ground penetrating radar (GPR) observations were gathered in an effort to delineate structural features and to map porosity variations. The radar measurements were obtained using a Sensors and Software pulseEKKO 100 ground penetrating radar system equipped with 200 MHz antennas. Data were gathered at source and receiver spacings of 0.25 m over an interval of 1 to 18 m in depth. Good signal quality was noted for all offsets, and first arrival times were picked from the GPR traces. Using the crosswell arrival times I constructed a model of the lateral variation in the radar velocity based upon an LSQR-based inversion method (Vasco *et al.* 1997). The velocity variations are converted to dielectric constant and are shown in Fig. 11. The range of values is appropriate for saturated sediments of varying degrees of coarseness (Telford *et al.* 1976, p. 456).

I modelled the waveforms associated with five receiver locations for a source situated at approximately 8 m in depth. The five trajectories from the source to the receivers are shown as curves in Fig. 11. The trajectories are found by solving the ray eqs (12a) and (12b) for γ [eq. (11)] which is based upon the variations shown in Fig. 11. For this first attempt at modelling the waveforms I have assumed a constant background variation in conductivity, σ. The frequency varied between 5 MHz and 200 MHz, with the trajectories in Fig. 11 corresponding to 200 MHz. The background conductivity was determined from the the decay of the root-mean-squared amplitude with offset (Fig. 12). Note that the amplitude decays by roughly 40 per cent over a distance of about 0.25 m. I fit this decay with distance

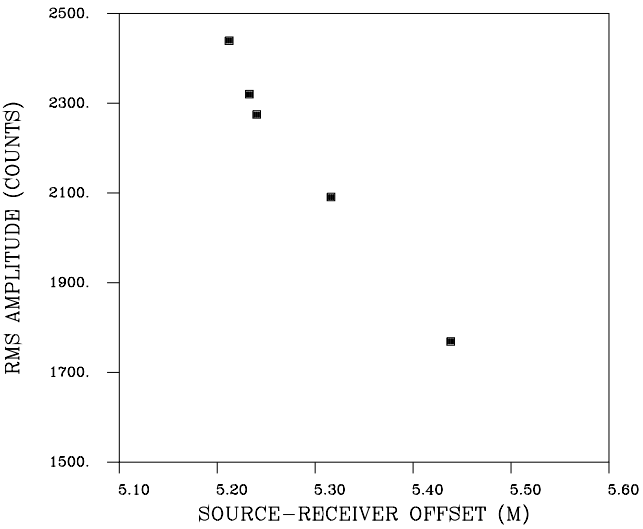

Figure 12. Root-mean-squared amplitude plotted as a function of offset from the source. The five points are associated with observations from the five receivers in the source gather. The source amplitude is given in digital counts.

to a simple exponential model,

$$\ln(E/A) - \ln(\sin\theta) + \ln(r) = -\alpha r$$

where E is the observed amplitude, A is the source amplitude, θ is the angle between the source and receiver, and r is the source-receiver offset, in order to estimate the slope α. From the slope I estimate the background conductivity to be 5.3×10^{-4} mhos m^{-1}, a resistivity of 1886.8 Ωm, a value which is consistent with that of various sediments (Telford *et al.* 1976, p. 455). I should note that for frequencies

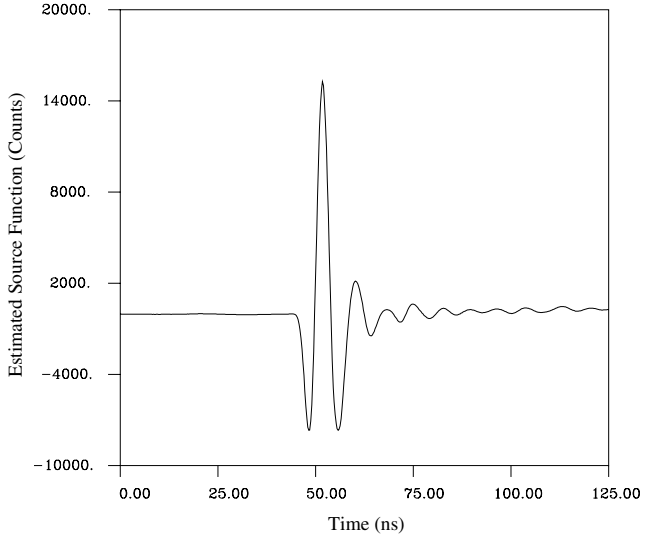

Figure 13. Source-time function which was deconvolved from the five observed GPR waveforms. The source amplitude is in digital counts.

between 5 and 200 MHz the ratio $\omega\varepsilon/\sigma$ varies from approximately 1 to 40, respectively. Hence, the wavefield contains components for which diffusion and wave-like propagation are approximately equal at 5 MHz, to a regime in which wave-like propagation dominates at 200 MHz.

In order to model the waveforms I first estimate a source-time function. The estimated source wavelet, deconvolved from the observed waveforms, is shown in Fig. 13. Note that the source-time function is similar to a Ricker wavelet, with the first two troughs roughly equal is magnitude. The propagation was modelled using the trajectory-based approach, described above, for 256 frequencies between 5 and 200 MHz. In particular, I use expression (22) to calculate the waveforms. The response of the medium is computed from the expressions for the complex phase $\varphi(\mathbf{s}_f)$ and the amplitude variation along the trajectory, eqs (13) and (16), respectively. The response functions for the five receivers are shown in Fig. 14. The final waveforms, obtained by convolving the source-time function with the response functions, is shown in Fig. 15, as a dashed line. For comparison, the observed GPR traces are also shown as solid lines. Overall, the agreement is fairly good, with the secondary trough having a slightly smaller amplitude than the first in both the observed and calculated traces.

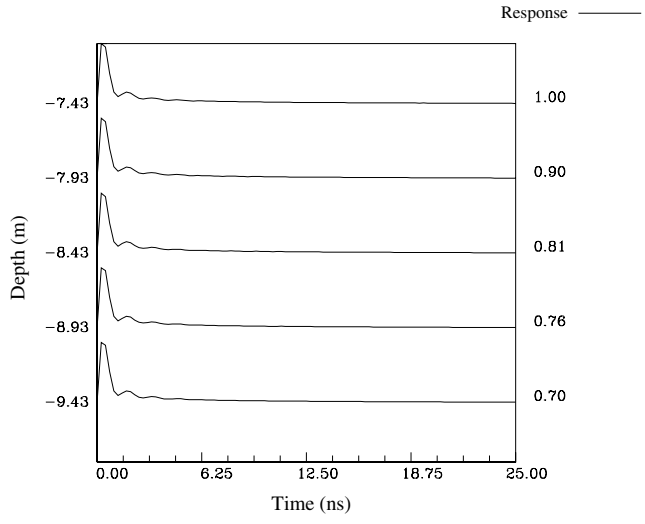

Figure 14. The response functions for the five receivers modelled in the experiment. The numbers on the right denote the relative amplitude of the response functions.

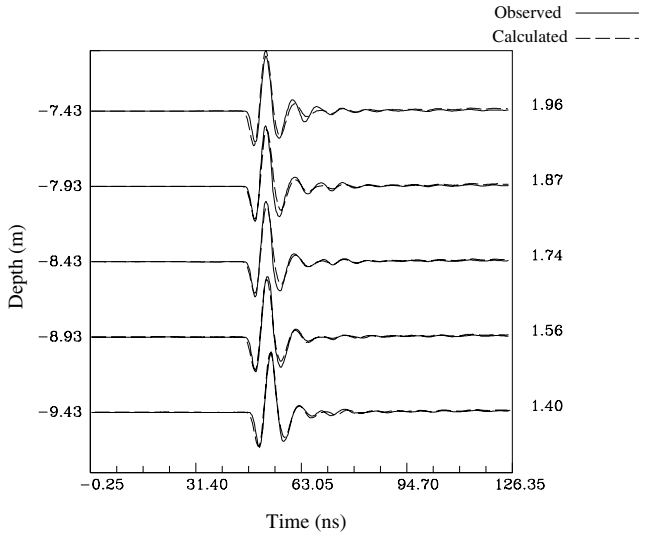

Figure 15. Observed (solid lines) and calculated (dashed lines) ground penetrating radar waveforms for the five receivers considered in this study. The numbers on the right denote the relative amplitude of the five sets of traces.

4 CONCLUSIONS

The method of multiple-scales provides a useful framework for modelling electromagnetic propagation within the Earth. The technique is very general and allows one to treat both wave-like and diffusive field propagation in a unified manner. It was shown that, in the limit, one recovers previously derived results which represent wave-like and diffusive behaviours. Furthermore, one can also model intermediate frequency propagation which cannot be described as either purely diffusive or purely wave-like. For the numerical illustration presented in this paper both conduction and displacement currents are found to be important between 10 and 100 MHz. The generality of the method of multiple-scales has been noted by others and it has been used to model hyperbolic, dispersive, diffusive, and nonlinear phenomena (Whitham 1974; Jeffrey & Kawahara 1982; Anile *et al.* 1993). It has proven useful in modelling fluid flow and transport when the problems are of mixed character, that is dispersive, diffusive and advective (Vasco & Finsterle 2004; Vasco 2004).

The semi-analytic expression for the electric field, eq. (18), should prove useful for inversion and imaging. The asymptotic methodology, on which the method of multiple-scales relies, partitions the inverse problem into one related to the phase or arrival time and another related to the amplitude (Kravtsov & Orlov 1990; Keller & Lewis 1995). This partitioning allows one to define an arrival time associated with a transient electromagnetic wavefield as noted by others (Virieux *et al.* 1994; Yu & Edwards 1997). The trajectory-based approach may also be used in conjunction with numerical simulation codes to formulate a hybrid inversion scheme (Vasco & Finsterle 2004).

This work is preliminary and can be extended in several respects. First, further testing is necessary to determine the limits of applicability of this approach. In particular, how smooth is the medium

© 2007 The Author, *GJI*, **168,** 949–963
Journal compilation © 2007 RAS

required to be in order for the technique to correctly model the wavefield? Also, the effects of boundaries and interfaces need to be incorporated into any practical modelling algorithm. Finally, the expressions derived here can be incorporated into an inversion scheme. Such an inversion algorithm should be rather efficient.

ACKNOWLEDGMENTS

I would like to thank Ki Ha Lee, Alex Becker and Lou Reginato for the use of the data from the experiment at the Richmond Field Station, California. I also thank John Peterson of Berkeley Laboratory for providing the ground penetrating radar observations from the Boise Hydrogeophysical Research Site experiment. This work was supported by the Assistant Secretary, Office of Basic Energy Sciences of the US Department of Energy under contract DE-AC03-76SF00098. All computations were carried out at the Center for Computational Seismology, Berkeley Laboratory.

REFERENCES

Aki, K. & Richards, P.G., 2002. *Quantitative Seismology*, University Science Books, Sausalito.

Amodei, D., Keers, H., Vasco, D. & Johnson, L., 2006. Computation of uniform wave forms using complex rays, *Physical Review E,* **73,** 036704/1-14.

Alumbaugh, D.L. & Morrison, H.F., 1995. Theoretical and practical considerations for crosswell electromagnetic tomography assuming a cylindrical geometry, *Geophysics,* **60,** 846–870.

Alumbaugh, D.L., Newman, G.A., Prevost, L. & Shadid, J.N., 1996. Three-dimensional wideband electromagnetic modelling on massively parallel computers, *Radio Science,* **31,** 1–23.

Anile, A.M., Hunter, J.K., Pantano, P. & Russo, G., 1993. *Ray Methods for Nonlinear Waves in Fluids and Plasmas*, Longman Scientific and Technical, New York.

Barker, R. & Moore, J., 1998. The application of time-lapse electrical tomography in groundwater studies, *The Leading Edge,* **17,** 1454–1458.

Becker, A., Lee, K.H. & Reginato, L., 1999. *Field Test of a Wideband Downhole EM Transmitter*, E. O. Lawrence Berkeley National Laboratory Report, LBNL-**43762**, Berkeley.

Binley, A., Winship, P., Middleton, R., Magdeline, P. & West, J., 2001. High-resolution characterization of vadose zone dynamics using cross-borehole radar, *Water Resources Research,* **37,** 2639–2652.

Borovikov, V.A. & Kinber, B.Y., 1994. *Geometrical Theory of Diffraction*, The Institution of Electrical Engineers, London.

Chew, W.C., 1995. *Waves and Fields in Inhomogeneous Media*, IEEE Press, New York.

Choudhary, S. & Felsen, L.R., 1973. Asymptotic theory for inhomogeneous waves, *IEEE Trans. Ant. Prop.,* **21,** 827–842.

Clement, W.P., Barrash, W. & Knoll, M.D., 2006. Reflectivity modelling of a ground-penetrating-radar profile of a saturated fluvial formation, *Geophysics,* **71,** K59–K66.

Coggon, J.H., 1971. Electromagnetic and electrical modelling by the finite element method, *Geophysics,* **36,** 132–155.

Cohen, J.K. & Lewis, R.M., 1967. A ray method for the asymptotic solution of the diffusion equation, *J. Inst. Maths. Applics.,* **3,** 266–290.

Courant, R. & Hilbert, D., 1962. *Methods of Mathematical Physics*, Interscience, New York.

Daily, W.D. & Lytle, R.J., 1983. Geophysical tomography, *J. Geomagn, Geoelectr.,* **35,** 423–442.

Davis, H.F., 1967. *Introduction to Vector Analysis*, Allyn and Bacon, Boston.

Davis, J.L. & Annan, A.P., 1989. Ground penetrating radar for high-resolution mapping of soil and rock stratigraphy, *Geophys. Prospect.,* **37,** 531–551.

Druskin, V. & Knizhnerman, L., 1994. A spectral approach to solving three-dimensional diffusion Maxwell's equations in the time and frequency domains, *Radio Science,* **29,** 937–953.

Egorchenkov, R.A. & Kravtsov, Y.A., 2001. Complex ray-tracing algorithms with applications to optical problems, *J. Opt. Soc. Am.,* **18,** 650–656.

Felsen, L.B., 1976. Evanescent waves, *J. Opt. Soc. Am.,* **66,** 751–760.

Frangos, W., Becker, A. & Lee, K.H., 2004. High-frequency and very-high-frequency (HF. & VHF) above-ground electromagnetic impedance measurements, *J. Env. Eng. Geophys.,* **9,** 87–93.

Gardner, C.S. & Morikawa, G.K., 1960. Similarity in the asymptotic behaviour of collision-free hydromagnetic waves and water waves, *Courant Inst. Math. Sci. Rep.,* **90,** 9082,1.

Gear, C.W., 1971. *Numerical Initial Value Problems in Ordinary Differential Equations*, Prentice-Hall, Englewood Cliffs, New Jersy.

Goodman, D., 1994. Ground-penetrating radar simulation in engineering and archaeology, *Geophysics,* **59,** 224–232.

Habashy, T.M., Groom, R.W. & Spies, B.R., 1993. Beyond the Born and Rytov approximations: A nonlinear approach to electromagnetic scattering, *J. geophys. Res.,* **98,** 1759–1775.

Hearn, D.J. & Krebes, E.S., 1990. On computing ray-synthetic seismograms for anelastic media using complex rays, *Geophysics,* **55,** 422–432.

Hohmann, G.W., 1971. Electromagnetic scattering by conductors in the Earth near a line source of current, *Geophysics,* **36,** 101–131.

Hoversten, G.M., Gritto, R., Washbourne, J. & Daley, T., 2003. Pressure and fluid saturation prediction in a multicomponent reservoir using combined seismic and electromagnetic imaging, *Geophysics,* **68,** 1580–1591.

Huisman, J.A., Hubbard, S.S., Redman, J.D. & Annan, A.P., 2003. Measuring soil water content with ground penetrating radar: A review, *Vadose Zone Journal,* **2,** 1–16.

Jeffrey, A. & Kawahara, T., 1982. *Asymptotic Methods in Nonlinear Wave Theory*, Pitman Advanced Publishing, Boston.

Keller, H.B., 1968. *Numerical Methods for Two-Point Boundary-Value Problems*, Blaisdell, Waltham, Ma.

Keller, J.B. & Lewis, R.M., 1995. Asymptotic methods for partial differential equations: The reduced wave equation and Maxwell's Equations, in *Surveys in Applied Mathematics*, Vol. 1, pp. 1–82, eds Keller, J.B., McLaughlin, D.W. & Papanicolaou, G.C., Plenum Press, New York.

Kline, M. & Kay, I.W., 1965. *Electromagnetic Theory and Geometrical Optics*, Robert E. Krieger Publishing, Huntington, NY.

Korsunsky, S., 1997. *Nonlinear Waves in Dispersive and Dissipative Systems with Coupled Fields*, Addison Wesley Longman, Essex.

Kravtsov, Y.A. & Orlov, Y.I., 1990. *Geometrical Optics of Inhomogeneous Media*, Springer-Verlag, Berlin.

Kravtsov, Y.A., Forbes, G.W. & Asatryan, A.A., 1999. Theory and applications of complex rays, in *Progress in Optics*, Vol., XXXIX, pp. 1–62, ed. Wolf, E., Elsevier, Amsterdam.

Lager, D.L. & Lytle, R.J., 1977. Determining a subsurface electromagnetic profile from high-frequency measurements by applying reconstruction-technique algorithms, *Radio Science,* **12,** 249–260.

Lee, K.H. & Xie, G., 1993. A new approach to imaging with low-frequency electromagnetic fields, *Geophysics,* **58,** 780–796.

Lee, T.J., Suh, J.H., Kim, H.J., Song, Y. & Lee, K.H., 2002. Electromagnetic traveltime tomography using an approximate wavefield transform, *Geophysics,* **67,** 68–76.

Lewis, R. M., 1965. Asymptotic theory of wave propagation, *Arch. Rat. Mech. Anal.,* **20,** 191.

Luneburg, R.K., 1966. *Mathematical Theory of Optics*, University of California Press, Berkeley.

Morrison, H.F., Phillips, R.S. & O'Brien, D.P., 1969. Quantitative interpretation of transient electromagnetic fields over a layered half-space, *Geophys. Prospect.,* **17,** 82–101.

Nekut, A.G., 1994. Electromagnetic ray-trace tomography, *Geophysics,* **59,** 371–377.

Newman, G.A. & Alumbaugh, D.L., 1995. Frequency-domain modelling of airborne electromagnetic responses using staggered finite differences, *Geophys. Prospect.,* **43,** 1021–1042.

Newman, G.A. & Commer, M., 2005. New advances in three dimensional transient electromagnetic inversion, *Geophys. J. Int.,* **160,** 5–32.

Newman, G.A., Hohmann, G.W. & Anderson, W.L., 1986. Transient electromagnetic response of a three-dimensional body in a layered earth, *Geophysics,* **51,** 1608–1627.

Olsson, O., Falk, L., Forslund, L., Lundmark, L. & Sandberg, E., 1992. Borehole radar applied to the characterization of hydraulically conductive fracture zones in crystalline rock, *Geophys. Prospect.,* **40,** 109–142.

Oristaglio, M.L. & Hohmann, G.W., 1984. Diffusion of electromagnetic fields in a two-dimensional Earth: A finite-difference approach, *Geophysics,* **49,** 870–894.

Parry, J.R., 1969. Integral Equation Formulations of Scattering from Two-Dimensional Inhomogeneities in a Conductive Earth, *PhD thesis,* University of California, Berkeley.

Peterson, J.E., 2001. Pre-inversion corrections and analysis of radar tomographic data, *J. Env. Eng. Geophys.,* **6,** 1–18.

Press, W.H., Teukolsky, S.A., Vetterling, W.T. & Flannery, B.P., 1992. *Numerical Recipes in Fortran*, Cambridge University Press, Cambridge.

Ryu, J., Morrison, H.F. & Ward, S.H., 1970. Electromagnetic fields about a loop source of current, *Geophysics,* **35,** 862–896.

Seckler, B.D. & Keller, J.B., 1959. Geometrical theory of diffraction in inhomogeneous media, *J. acoust. Soc. Am.,* **31,** 192–205.

Silvester, P. & Haslam, C.R.S., 1972. Magnetotelluric modelling by the finite element method, *Geophys. Prospect.,* **20,** 872–891.

Spies, B.R. & Habashy, T.M., 1995. Sensitivity analysis of crosswell electromagnetics, *Geophysics,* **60,** 834–845.

Stewart, D.C., Anderson, W.L., Grover, T.P. & Labson, V.F., 1994. Shallow subsurface mapping by electromagnetic sounding in the 300 kHz to 30 MHz range: Model studies and prototype system assessment, *Geophysics,* **59,** 1201–1210.

Telford, W.M., Geldart, L.P., Sheriff, R.E. & Keys, D.A., 1976. *Applied Geophysics*, Cambridge University Press, Cambridge.

Tikhonov, A.N., 1965. Mathematical basis of the theory of electromagnetic soundings, *USSR Comput. Math. and Math. Phys.,* **5,** 207–211.

Torres-Verdin, C. & Habashy, T.M., 1994. Rapid 2.5-D forward modelling and inversion via a new nonlinear scattering approximation, *Radio Science,* **29,** 1051–1079.

Tripp, A.C. & Hohmann, G.W., 1984. Block diagonalization of the electromagnetic impedance matrix of a symmetric buried body using group theory, *IEEE Trans. Geosci. Remote Sens.,* **22,** 62–69.

Vasco, D.W., 2004. An asymptotic solution for two-phase flow in the presence of capillary forces, *Water Resources Research,* **40,** W12407, 1–13.

Vasco, D.W. & Finsterle, S., 2004. Numerical trajectory calculations for the efficient inversion of transient flow and tracer observations, *Water Resources Research,* **40,** W01507, 1–17.

Vasco, D.W., Peterson, J.E. & Lee, K.H., 1997. Ground-penetrating radar velocity tomography in heterogeneous and anisotropic media, *Geophysics,* **62,** 1758–1773.

Vasco, D.W., Keers, H. & Karasaki, K., 2000. Estimation of reservoir properties using transient pressure data: An asymptotic approach, *Water Resources Research,* **36,** 3447–3465.

Virieux, J., Flores-Luna, C. & Gibert, D., 1994. Asymptotic theory for diffusive electromagnetic imaging, *Geophys. J. Int.,* **119,** 857–868.

Wait, J.R., 1954. Mutual coupling of loops lying on the ground, *Geophysics,* **19,** 290–296.

Whitham, G.B., 1974. *Linear and Nonlinear Waves*, Wiley, New York.

Yu, L. & Edwards, R.N., 1997. On crosswell diffusive time-domain electromagnetic tomography, *Geophys. J. Int.,* **130,** 449–459.

APPENDIX A: THE METHOD OF MULTIPLE SCALES

In this appendix I use the method of multiple scales to derive a trajectory-based solution to Maxwell's equations. The solution is valid when the heterogeneity is smoothly varying. In particular, the spatial variation in medium properties, is smooth with respect to the change in the electromagnetic field as the disturbance propagates through the subsurface. By spatial variation in medium properties I mean the scale length over which $\sigma(\mathbf{x})$, and $\varepsilon(\mathbf{x})$ vary. The scale length associated with a propagating electromagnetic wave is defined across the wave front and represents the distance over which the electric field changes from the background or initial value to the amplitude of the propagating disturbance. In the method of multiple scales, the scale length associated with the variation in medium properties is assumed to be much larger than the scale length of the propagating electromagnetic disturbance. If I denote the scale of variation of the background properties by L and the mean length of the variation across the propagating front by l, then $L \gg l$. The ratio of scales is characterized by the parameter $\epsilon = l/L$ which is assumed to be much smaller than 1.

In the method of multiple scales one defines slow variables $\mathbf{X}$ and T in terms of the physical variables $\mathbf{x}$ and t by

$$X^i = \epsilon x^i, \tag{A1a}$$

and

$$T = \epsilon t, \tag{A1b}$$

where $\epsilon = l/L$. The electric field is then written as a formal power series expansion in ϵ

$$\mathbf{E}(\mathbf{X}, \theta) = \sum_{p=0}^{\infty} \epsilon^p \mathbf{E}_p = e^{i\theta} \sum_{p=0}^{\infty} \epsilon^p \mathbf{A}_p(\mathbf{X}), \tag{A2}$$

where $\theta(\mathbf{x})$ is the local phase. The local phase is a rapidly varying quantity, or fast variable, which may be written in terms of a slowly varying quantity, $\theta(\mathbf{x})$,

$$\theta(\mathbf{x}) = \frac{1}{\epsilon}\Theta(\mathbf{X}). \tag{A3}$$

The series (A2) may be thought of as a local plane wave expansion.

Now $\mathbf{E}(\mathbf{X}, \theta)$ depends on $\mathbf{x}$ through the dependence of $\mathbf{X}$ and θ on $\mathbf{x}$. Thus, the partial derivatives which appear in the vector differential eq. (7) may be rewritten in terms of the new variables. For example, the partial derivative with respect to t is given by

$$\frac{\partial}{\partial t} = \epsilon \frac{\partial}{\partial T} + \frac{\partial \theta}{\partial T}\frac{\partial}{\partial \theta}. \tag{A4a}$$

and similarly for the partial derivative with respect to x_i

$$\frac{\partial}{\partial x_i} = \epsilon \frac{\partial}{\partial X_i} + \frac{\partial \theta}{\partial X_i}\frac{\partial}{\partial \theta}. \tag{A4b}$$

Based upon (A4a) I can write the vector differential curl operator in (7) as

$$\nabla \times \mathbf{E} = \epsilon \nabla_X \times \mathbf{E} + \nabla\theta \times \frac{\partial \mathbf{E}}{\partial \theta}, \tag{A5}$$

where ∇_X signifies the gradient with respect to the slow variables $\mathbf{X}$.

The vector differential eq. (7) may be written in terms of the new variables and the corresponding transformed operators.

$$\begin{aligned}
&\epsilon^2 \nabla_X \times \mu^{-1}\nabla_X \times \mathbf{E} + \epsilon \nabla_X \times \mu^{-1}\nabla\theta \times \frac{\partial \mathbf{E}}{\partial \theta} \\
&\quad + \epsilon \nabla\theta \times \mu^{-1}\nabla_X \times \frac{\partial \mathbf{E}}{\partial \theta} + \nabla\theta \times \mu^{-1}\nabla\theta \times \frac{\partial^2 \mathbf{E}}{\partial \theta^2} \\
&\quad + \varepsilon \left[\epsilon^2 \frac{\partial^2 \mathbf{E}}{\partial T^2} + \epsilon \frac{\partial^2 \theta}{\partial T^2}\frac{\partial \mathbf{E}}{\partial \theta} + 2\epsilon \frac{\partial \theta}{\partial T}\frac{\partial^2 \mathbf{E}}{\partial T \partial \theta} + \frac{\partial \theta}{\partial T}\frac{\partial \theta}{\partial T}\frac{\partial^2 \mathbf{E}}{\partial \theta^2} \right] \\
&\quad + \sigma \left[\epsilon \frac{\partial \mathbf{E}}{\partial T} + \frac{\partial \theta}{\partial T}\frac{\partial \mathbf{E}}{\partial \theta} \right] = 0.
\end{aligned} \tag{A6}$$

Note that, from the specific form for $\mathbf{E}$, eq. (A2), the n-th partial derivative with respect to θ reduces to

$$\frac{\partial^n \mathbf{E}}{\partial \theta^n} = (-i)^n \mathbf{E}. \tag{A7}$$

© 2007 The Author, *GJI*, **168,** 949–963
Journal compilation © 2007 RAS

Thus, eq. (A6) takes the form

$$\epsilon^2 \nabla_X \times \mu^{-1} \nabla_X \times \mathbf{E} + i\epsilon \nabla_X \times \mu^{-1} \nabla\theta \times \mathbf{E} + i\epsilon \nabla\theta \times \mu^{-1} \nabla_X \times \mathbf{E} - \nabla\theta \times \mu^{-1} \nabla\theta \times \mathbf{E} + \varepsilon \left[\epsilon^2 \frac{\partial^2 \mathbf{E}}{\partial T^2} + \epsilon \mathrm{i} \frac{\partial^2 \theta}{\partial T^2} \mathbf{E} + 2\epsilon \mathrm{i} \frac{\partial \theta}{\partial T} \frac{\partial \mathbf{E}}{\partial T} - \frac{\partial \theta}{\partial T} \frac{\partial \theta}{\partial T} \mathbf{E} \right] + \sigma \left[\epsilon \frac{\partial \mathbf{E}}{\partial T} + \mathrm{i} \frac{\partial \theta}{\partial T} \mathbf{E} \right] = 0. \tag{A8}$$

Substituting the series expansion (A2) for **E** produces an expression which contains terms of various orders in ϵ. Because ϵ is assumed to be small, the lowest order terms are the most significant. In the following subsections I shall consider terms of order ϵ^0 and ϵ^1.

A1 Terms of order ϵ^0

Considering only terms of order $\epsilon^0 \sim 1$, from eq. (A8) I arrive at an equation for the phase $\theta(\mathbf{X}, T)$

$$\nabla\theta \times \nabla\theta \times \mathbf{A}_0 + \left[\mu\varepsilon \frac{\partial \theta}{\partial T} \frac{\partial \theta}{\partial T} - i\mu\sigma \frac{\partial \theta}{\partial T} \right] \mathbf{A}_0 = 0. \tag{A9}$$

Because $\partial\,\theta/\partial T$ is never zero, I may write the phase function in the partitioned form (Kline & Kay 1965, p. 50)

$$\theta(\mathbf{X}, T) = \omega T - \varphi(\mathbf{X}) \tag{A10}$$

where $\varphi(\mathbf{X})$ depends implicitly upon ω. Using the definition

$$\mathbf{p} = \nabla\varphi, \tag{A11}$$

I can re-write (A9) as

$$[\mathbf{p} \times \mathbf{p} \times \mathbf{I} + \gamma \mathbf{I}]\, \mathbf{A}_0 = 0 \tag{A12}$$

where

$$\gamma = \mu\omega(\omega\varepsilon - i\sigma). \tag{A13}$$

Using the vector cross-product identity

$$\mathbf{p} \times \mathbf{p} \times \mathbf{I} = (\mathbf{p} \cdot \mathbf{I})\mathbf{p} - p^2 \mathbf{I}$$

(Davis 1967, p. 46), where I have defined

$$p^2 = \mathbf{p} \cdot \mathbf{p}, \tag{A14}$$

eq. (A12) becomes

$$[(p^2 - \gamma)\mathbf{I} - \mathbf{p}\mathbf{p}^T]\mathbf{A}_0 = 0. \tag{A15}$$

For eq. (A15) to have a non-trivial solution for $\mathbf{A}_0$, the determinant of the coefficient matrix must vanish

$$\det[(p^2 - \gamma)\mathbf{I} - \mathbf{p}\mathbf{p}^T] = 0. \tag{A16}$$

Expanding the determinant produces the following polynomial equation for p

$$\gamma(p^2 - \gamma)^2 = 0. \tag{A17}$$

Eq. (A17) has three roots, $\gamma = 0$ and $(p^2 - \gamma)^2 = 0$. I am interested in the physical solution which decays with distance from the source. Thus, I take the root of $(p^2 - \gamma)^2 = 0$ which corresponds to a decaying wave. Because $p^2 = \mathbf{p} \cdot \mathbf{p}$, the root $p^2 - \gamma = 0$ is equivalent to the condition

$$\mathbf{p} \cdot \mathbf{p} = \gamma. \tag{A18}$$

Upon using the definition (A11), I arrive at the eikonal equation

$$\nabla\varphi \cdot \nabla\varphi = \gamma, \tag{A19}$$

a non-linear partial differential equation governing the evolution of φ.

It is well known (Courant & Hilbert 1962) that the eikonal eq. (A19) is equivalent to a system of ordinary differential equations, the ray equations (Kravtsov & Orlov 1990, p. 12)

$$\frac{d\mathbf{s}}{ds} = \frac{1}{\sqrt{\gamma}} \mathbf{p} \tag{A20}$$

$$\frac{d\mathbf{p}}{ds} = \nabla\sqrt{\gamma}$$

where $\mathbf{s}\,(s)$ is the 'ray', a path through the model, and s is a parameter signifying the distance along the ray. Eqs (A20) may be solved numerically, yielding both the trajectory through the model $\mathbf{s}(s)$ and the gradient of the phase $\mathbf{p}(s)$. By writing the equation for the phase (A19) in ray coordinates, I can derive an expression for φ as an integral along the ray path,

$$\varphi(s_f) = \int_{s_0}^{s_f} \sqrt{\gamma}\, ds \tag{A21}$$

where s_0 is the initial point along the ray path and s_f is the final observation point.

Note that γ, defined by (A13) is generally complex, leading to complex ray equations. Furthermore, the ray equations depend upon ω and must be solved for each frequency of interest. In situations in which only a small number of frequencies are of interest, for example, for a frequency-domain inversion, this attribute may be used to some advantage. That is, one can limit the work to computations associated with the required frequencies.

A2 Terms of order ϵ^1

If I consider terms of order ϵ in eq. (A8), after substituting in the series expansion (A2) for **E** I find

$$i\nabla_X \times \mu^{-1}\mathbf{p} \times \mathbf{E}_0 + i\mathbf{p} \times \mu^{-1}\nabla_X \times \mathbf{E}_0 + i\eta \frac{\partial \mathbf{E}_0}{\partial T} + \varepsilon i \frac{\partial^2 \theta}{\partial T^2} \mathbf{E}_0 + \mathbf{p} \times \mu^{-1}\mathbf{p} \times \mathbf{E}_1 + \gamma \mathbf{E}_1 = 0 \tag{A22}$$

where

$$\eta = 2\omega\varepsilon - i\sigma.$$

Note that, in light of the definition (A10), the second partial derivative of θ with respect to time in (A22) vanishes. Because of (A12), the terms containing $\mathbf{E}_1$ vanish and eq. (A22) reduces to

$$\mu\eta \frac{\partial \mathbf{E}_0}{\partial T} + \nabla_X \times \mathbf{p} \times \mathbf{E}_0 + \mathbf{p} \times \nabla_X \times \mathbf{E}_0 = 0. \tag{A23}$$

Next I use vector identities (Davis 1967, p. 116) to write (A23) as a set of coupled vector transport equations

$$\mu\eta \frac{\partial \mathbf{E}_0}{\partial T} - 2\,(\mathbf{p} \cdot \nabla)\,\mathbf{E}_0 + (\nabla \cdot \mathbf{E}_0)\,\mathbf{p} - (\nabla \cdot \mathbf{p})\,\mathbf{E}_0 = 0 \tag{A24}$$

governing the evolution of the field vector $\mathbf{E}_0$. By writing the vector transport equation in characteristic coordinates $\mathbf{p}/\sqrt{\gamma}$ I may reduce (A24) to the system of partial differential equations

$$\mu\eta \frac{\partial \mathbf{E}_0}{\partial T} - 2\frac{\partial \mathbf{E}_0}{\partial s} - (\nabla \cdot \mathbf{E}_0)\,\mathbf{p} + (\nabla \cdot \mathbf{p})\,\mathbf{E}_0 = 0 \tag{A25}$$

where s denotes the distance along the trajectory $\mathbf{s}(s)$. Because of the particular dependence on T as specified in eqs (A2) and (A10) eq. (A25) may be written

$$2\frac{\partial \mathbf{E}_0}{\partial s} + (\nabla \cdot \mathbf{E}_0)\,\mathbf{p} - (\nabla \cdot \mathbf{p} + \mu\eta\omega i)\,\mathbf{E}_0 = 0. \tag{A26}$$

I can re-write (A26) as a differential equation for the squared field amplitude upon taking the scalar product with $\mathbf{E}_0$ and noting that $\mathbf{E}_0 \cdot \mathbf{p}$ vanishes and

$$2\frac{\partial \mathbf{E}_0}{\partial s} \cdot \mathbf{E}_0 = \frac{\partial {E_0}^2}{\partial s}. \tag{A27}$$

Only the derivative with respect to s remains after taking the dot product with $\mathbf{E}_0$ and eq. (A26) may then be written as an ordinary differential equation

$$\frac{d{E_0}^2}{ds} + \Psi(s){E_0}^2 = 0, \tag{A28}$$

where

$$\Psi(s) = \nabla \cdot \mathbf{p} + \mu\omega\sigma + 2\mu\omega^2\varepsilon i. \tag{A29}$$

Eq. (A28) may be integrated to give

$${E_0}^2(s) = {E_0}^2(s_0)\exp\left\{-\int_{s_0}^{s}\Psi(s)\,ds\right\}. \tag{A30}$$

Because $\Psi(s)$ depends upon frequency, the field amplitude will generally be frequency-dependent. This equation is similar in form to the transport equations derived by Kline & Kay (1965, p. 188) and Kravtsov & Orlov (1990, p. 22) for high frequency electromagnetic wave propagation.

© 2007 The Author, *GJI*, **168,** 949–963
Journal compilation © 2007 RAS